Geophysical Research Letters

RESEARCH LETTER
10.1029/2025GL116967

Depth Fluctuations of Mediterranean Outflow Water Along Its Northward Propagation During the Late Pleistocene

Xinyang Chen[1], Jiawang Wu[1,2], Xiaolei Pang[3], Haowen Dang[4], Lifeng Zhong[1], Jimin Yu[5,6], Christophe Colin[7], Zhifei Liu[4], Gert J. de Lange[8], Stefanie Kaboth-Bahr[9], Chuang Xuan[10], Hisashi Ikeda[11], Timothy D. Herbert[12], Huai-Hsuan May Huang[13], Carlos A. Alvarez Zarikian[14], Fátima F. G. Abrantes[15,16], and David A. Hodell[17]

[1]School of Marine Sciences, Sun Yat-Sen University and Southern Marine Science and Engineering Guangdong Laboratory (Zhuhai), Zhuhai, China, [2]Guangdong Provincial Key Laboratory of Marine Resources and Coastal Engineering, Guangzhou, China, [3]School of Ocean Sciences, China University of Geosciences (Beijing), Beijing, China, [4]State Key Laboratory of Marine Geology, Tongji University, Shanghai, China, [5]Laoshan Laboratory, Qingdao, China, [6]Research School of Earth Sciences, Australian National University, Canberra, ACT, Australia, [7]GEOPS, CNRS, Université Paris-Saclay, Orsay, France, [8]Department of Earth Sciences, Utrecht University, Utrecht, The Netherlands, [9]Institute of Geological Sciences, Freie Universität Berlin, Berlin, Germany, [10]School of Ocean and Earth Science, University of Southampton, Southampton, UK, [11]Geosphere Sciences, Yamaguchi University, Yamaguchi, Japan, [12]Department of Earth, Environmental and Planetary Sciences, Brown University, Providence, RI, USA, [13]Department of Geosciences, Princeton University, Princeton, NJ, USA, [14]International Ocean Discovery Program, Texas A&M University, College Station, TX, USA, [15]Portuguese Institute of the Sea and Atmosphere (IPMA), Lisbon, Portugal, [16]Centre of Marine Sciences (CCMAR/CIMAR LA), University of Algarve, Faro, Portugal, [17]Department of Earth Sciences, University of Cambridge, Cambridge, UK

Key Points:

- Sortable silt serves as a robust proxy to infer the flow speed of Mediterranean Outflow Water (MOW) on the Iberian Margin
- MOW shoaled during interglacials compared to glacials, and its deepening coincided with the prevalence of millennial climate variability
- Downstream MOW's depth variations were paced by precession, being deeper at precession maxima when its flow intensified

Supporting Information:

Supporting Information may be found in the online version of this article.

Correspondence to:

J. Wu,
wujiaw5@mail.sysu.edu.cn

Citation:

Chen, X., Wu, J., Pang, X., Dang, H., Zhong, L., Yu, J., et al. (2025). Depth fluctuations of Mediterranean Outflow Water along its northward propagation during the late Pleistocene. *Geophysical Research Letters*, *52*, e2025GL116967. https://doi.org/10.1029/2025GL116967

Received 12 MAY 2025
Accepted 25 JUN 2025

Author Contributions:

Conceptualization: Jiawang Wu
Data curation: Huai-Hsuan May Huang, Carlos A. Alvarez Zarikian
Formal analysis: Xinyang Chen, Jiawang Wu
Funding acquisition: Jiawang Wu, Xiaolei Pang, Lifeng Zhong, Jimin Yu
Investigation: Xinyang Chen
Methodology: Jiawang Wu
Project administration: Jiawang Wu, Carlos A. Alvarez Zarikian, Fátima F. G. Abrantes, David A. Hodell
Resources: Jiawang Wu, Xiaolei Pang, Haowen Dang, Lifeng Zhong, Jimin Yu, Christophe Colin, Zhifei Liu
Supervision: Jiawang Wu, Xiaolei Pang

Abstract Mediterranean Outflow Water (MOW) critically influences the Atlantic Meridional Overturning Circulation, yet its northward transport dynamics along the Iberian Margin remain unclear. Using terrigenous grain-size sortable silt and benthic foraminiferal carbon isotopes from two depth-strategic sites (U1389: 644 m vs. U1588: 1,339 m), we constrain MOW's northward depth fluctuations over the last 250 kyr. Results show that MOW progressively deepened from ~100 to 60 ka, then stabilized—synchronized with the prevalence of millennial-scale climate variability. During interglacials, MOW directly influenced U1588, while deepened below this site during glacials. Flow speed gradients between Sites U1389 and U1588 show pronounced precession cycles. At precession maxima—Northern Hemisphere summer insolation minima—when flow intensified, MOW underwent enhanced mixing and dilution during northward transport. This results from increased density contrasts between MOW and ambient waters, indicating deeper MOW penetration. We demonstrate precessional forcing on both the strength and depth of MOW's northward propagation.

Plain Language Summary The saline-warm Mediterranean Outflow Water (MOW) plays a crucial role in Atlantic Ocean circulation dynamics. Although precession-driven MOW strength variability has been documented, its depth variations during northward transport are poorly known. Here, we analyzed terrigenous grain-size sortable silt and benthic foraminiferal carbon isotopes from IODP Site U1588 on the Iberian Margin. Using data from two sites at diagnostic locations and depths along MOW's pathway, we develop a unified framework of hydrodynamic proxies to constrain MOW's depth fluctuations over the last 250 kyr. Results reveal that MOW gradually deepened from ~100 to 60 ka and then stabilized, coinciding with the development of millennial-scale climate variability. This deepening results from reduced North-Atlantic water density due to massive Heinrich Stadials meltwater discharges, and/or enhanced production of denser MOW driven by Mediterranean cooling/aridification. During interglacials, MOW shoaled and directly influenced U1588 sediments, while it sank below this site during glacials. MOW's depth variations closely follow precession cyclicity, being deeper during Northern Hemisphere summer insolation minima when flow intensified. This is because intensified MOW enhances the mixing and dilution as it moves northward, due to increased density contrasts with ambient waters. Our findings highlight precessional control over both the strength and depth of MOW's northward propagation.

Validation: Stefanie Kaboth-Bahr, Chuang Xuan, Hisashi Ikeda
Visualization: Xinyang Chen, Jiawang Wu
Writing – original draft: Xinyang Chen, Jiawang Wu
Writing – review & editing: Xinyang Chen, Jiawang Wu, Xiaolei Pang, Haowen Dang, Lifeng Zhong, Jimin Yu, Christophe Colin, Zhifei Liu, Gert J. de Lange, Stefanie Kaboth-Bahr, Chuang Xuan, Hisashi Ikeda, Timothy D. Herbert, Huai-Hsuan May Huang, Carlos A. Alvarez Zarikian, Fátima F. G. Abrantes, David A. Hodell

1. Introduction

The Mediterranean Outflow Water (MOW), a saline and warm water mass originating from the Mediterranean Sea, plays a key role in Atlantic Ocean circulation dynamics (Baringer & Price, 1997; Reid, 1979). Upon exiting through the Strait of Gibraltar, this dense water mass sinks to intermediate depths in the Gulf of Cadiz and subsequently flows northward along the Iberian Margin, where it bifurcates into upper and lower branches (Millot, 2009; Sánchez-Leal et al., 2017). With the prevailing depths of ∼300–800 m and ∼1,100–1,500 m respectively, these branches are characterized by a thermal contrast of ∼1.5–3.5°C but similar high salinity (∼38.5 psu) (Baringer & Price, 1997; Millot, 2009). Its northward progression, extending as far as 55°N, is governed by density gradients relative to ambient North Atlantic waters (Copard et al., 2011; Dubois-Dauphin et al., 2017; Lozier & Stewart, 2008; Reid, 1979). Specifically, as MOW moves northward, the continuous interaction with the surrounding water masses not only determines the depth of MOW itself, but also alters the properties of these waters (Figure 1).

As a result, MOW is thought to boost the Atlantic Meridional Overturning Circulation (AMOC) (Lozier & Stewart, 2008; Reid, 1979), and stabilize North Atlantic climate over the Pleistocene (Rogerson et al., 2012). Today, without the injection of MOW, the AMOC could slow down by ∼15% (W. Wu et al., 2007). The proposed mechanisms involve facilitating North Atlantic Deep Water (NADW) formation (Bigg et al., 2003; Lozier & Stewart, 2008; Swingedouw et al., 2019) and/or altering intermediate Atlantic thermal structure (Bower et al., 2002; Catunda et al., 2021; Ivanovic et al., 2014). However, key aspects of MOW variability remain unclear, particularly its prevailing depth and transport pathway across different timescales and climate cycles.

On millennial timescale, MOW is highly sensitive to changes in the Northern Hemisphere climate. During Heinrich Events that are characterized by massive iceberg discharge and melting in the North Atlantic and consequently a reduced NADW formation, MOW can, in turn, counteract this trend (Sierro et al., 2020; van Dijk et al., 2018; Voelker et al., 2006). By injecting salt and heat at intermediate depths into the delicately balanced, non-linear system of North Atlantic, this process could modulate the mode switch and intensity variations of AMOC (Bigg et al., 2003; Ivanovic et al., 2014).

In contrast, the orbital variability of MOW is determined by low-latitude climate processes. This is evidenced by the strong inverse correlation between MOW strength and African monsoon intensity in precession cycles (Bahr et al., 2015; Kaboth et al., 2016; McCave, 2023). A weak MOW is the direct consequence of increased runoff into the Mediterranean Sea during Northern Hemisphere summer insolation maxima, which inhibits the formation of Levantine Intermediate Water (LIW), the precursor of MOW (Colin et al., 2021; Rohling et al., 2015; J. Wu et al., 2019). Theoretically, hydraulic control of Gibraltar exchange should render MOW highly responsive to sea-level changes (Rogerson et al., 2005, 2012). However, its glacial-interglacial variability is barely distinguishable in marine sediment records. This discrepancy has sparked interest in proxy applicability. Epibenthic foraminiferal assemblages and $\delta^{13}C$ records suggest MOW was intensified during interglacial compared to glacial periods (Guo et al., 2017, 2020); while other proxy records from the same region show either temporally varied (Kaboth et al., 2017), absent (McCave, 2023), or even reversed (Nichols et al., 2020) glacial-interglacial patterns.

Apart from the proxy issues, possible vertical fluctuations of MOW present significant challenges for tracking its northward transport. Previous MOW-related studies focused on the Gulf of Cadiz, where a strong precessional imprint of MOW variability has been observed (Bahr et al., 2015). This is exemplified by International Ocean Discovery Program (IODP) Site U1389 at a water depth of 644 m (McCave, 2023). However, once MOW flows northward along the Iberian Margin, it tends to be deeper with greater variability, modulated by Atlantic density stratification (Rogerson et al., 2012)—especially during Marine Isotope Stage (MIS) 3 when Mediterranean buoyancy loss significantly changed (Cacho et al., 2006; Toucanne et al., 2007; Voelker et al., 2006). The most compelling evidence for this depth migration comes from the environmental magnetism data at Site U1391. These data show varying directions of bottom currents, indicating that the north-flowing MOW was sometimes above and sometimes below the 1,085 m water depth of Site U1391 (Nichols et al., 2020).

To fill these research gaps, we introduce a novel dual-site, single-proxy comparative approach. We use two strategically located sites at distinct depth ranges (U1389: 644 m vs. U1588: 1,339 m) along the northward pathway of MOW, implementing a unified framework based on sortable silt (SS) for bottom-current strength reconstruction (Figure 1). Terrigenous, non-cohesive SS is a robust hydrodynamic proxy for estimating near-bottom flow speed in deep-sea environments (McCave et al., 1995, 2017), with demonstrated success in

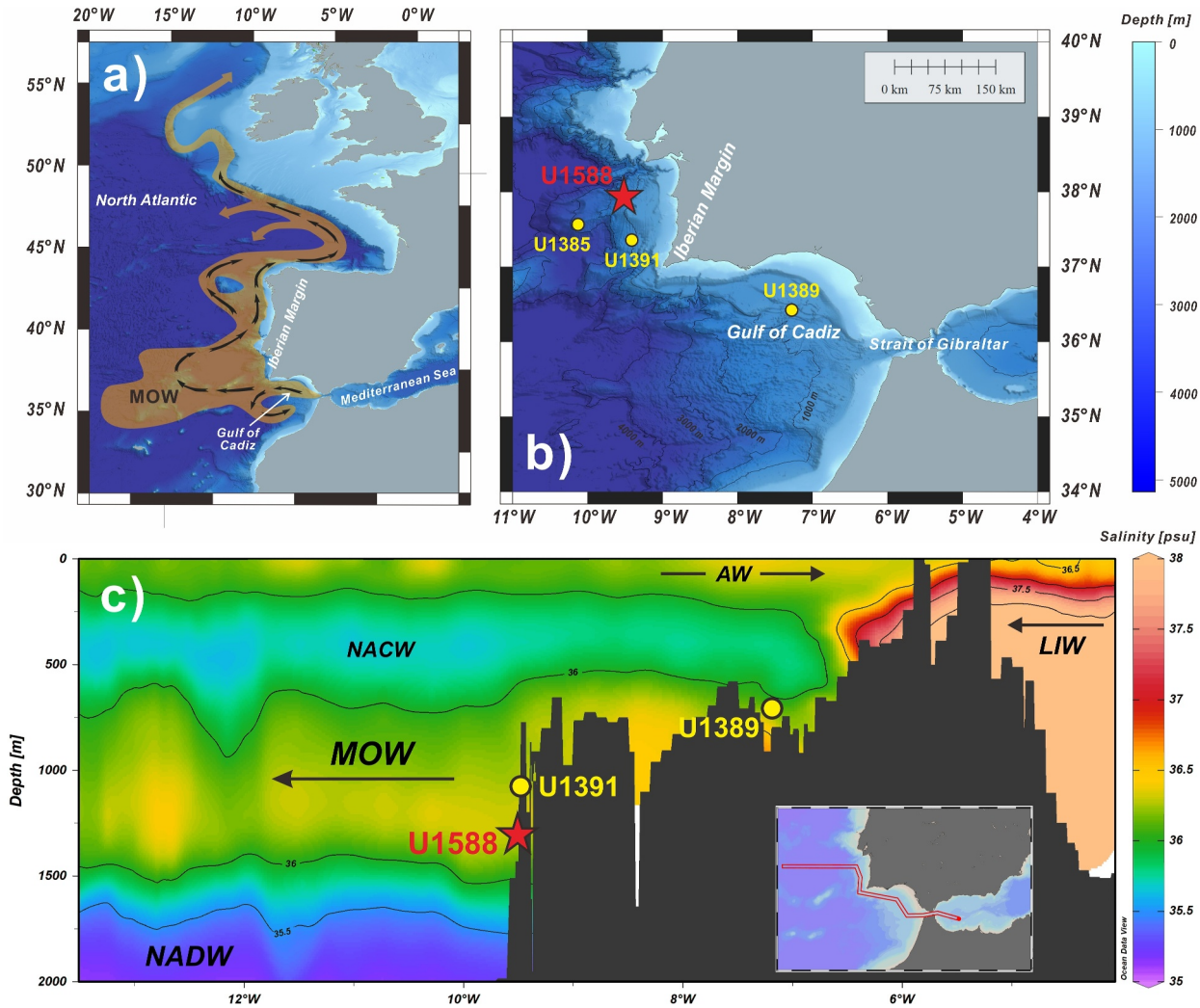

Figure 1. Spatial distribution of the Mediterranean Outflow Water (MOW), showing the locations of studied Site U1588, and other IODP sites mentioned in the main text. (a) MOW's northward transport pathways in the North Atlantic (modified after Iorga & Lozier, 1999). (b) Bathymetric map showing Site U1389 in the Gulf of Cadiz, and Sites U1391, U1385, and U1588 on the Iberian Margin. (c) Salinity profile reveals a distinct tongue along MOW's flow pathway, from the western Mediterranean through the Strait of Gibraltar and Gulf of Cadiz to the Iberian Margin, where its descending branch directly influences Site U1588. Legend for water masses: AW (Atlantic Water) = surface inflow to Mediterranean; LIW (Levantine Intermediate Water) = precursor of MOW in Mediterranean; MOW (Mediterranean Outflow Water); NACW (North Atlantic Central Water); NADW (North Atlantic Deep Water). The images were created using the Ocean Data View software (Schlitzer, 2022) with WOA18 salinity data (Zweng et al., 2018).

reconstructing MOW variations at Site U1389 (McCave, 2023). We present new SS data derived from grain-size analysis at Site U1588 on the Iberian Margin, complemented by benthic foraminiferal stable isotopes records over the last 250 kyr. This integrated setup enables us to (a) reconstruct MOW's depth and strength variations spanning the past two glacial-interglacial cycles, and (b) provide new constraints on the complex spatiotemporal dynamics of MOW along its northward transport.

2. Material and Methods

Site U1588 (37°57.61′N, 9°30.9′W; 1,339 m water depth) located on the southwestern Iberian Margin was recovered during IODP Expedition 397 (Hodell et al., 2024). It lies at a drift deposit shaped by the lower MOW branch (Abrantes et al., 2024; Hernández-Molina et al., 2014) (Figure 1b). The hydrodynamic linkages between compared sites is confirmed by modern seawater profile along MOW's transport pathway (Figure 1c): a high-salinity tongue traces the descending branch of MOW across the Strait of Gibraltar and Gulf of Cadiz (U1389: 644 m), and flowing along the Iberian Margin (U1391: 1,085 m; U1588: 1,339 m) into the northeastern Atlantic.

All analyses were performed on the same set of 90 samples, taken at ~60-cm spacing from 0.40 to 54.82 m composite depth of Site U1588, as described below. For full methodological details see Supporting Information S1.

Stable isotopes of oxygen ($\delta^{18}O$) and carbon ($\delta^{13}C$) were measured on 2–4 shells of benthic foraminifera from the >150 μm size fraction. We used mostly *Cibicidoides wuellerstorfi*, and occasionally *Cibicidoides mundulus*. When specimens of epifaunal *Cibicidoides* spp. were absent, *Uvigerina peregrina* were used, following Hodell et al. (2023). For different species, $\delta^{18}O$ and $\delta^{13}C$ values were corrected following Shackleton et al. (2000). Analytical procedures followed the protocol of Cheng et al. (2005).

The age model was constructed using three radiocarbon (^{14}C) dates on sea surface-dwelling planktonic foraminifera (Table S1 in Supporting Information S1), and by correlating benthic foraminiferal $\delta^{18}O$ with the global reference LR04 (Lisiecki & Raymo, 2005) (Figures S1 and S2 in Supporting Information S1). It suggests a bottom age of ~248.4 ka for the study interval, with mean sedimentation rate of ~22 cm/kyr and sampling resolution of ~2.8 kyr (Figure S3 in Supporting Information S1).

Isolation of terrigenous detrital particles followed the procedure of J. Wu et al. (2017). Grain size was analyzed on a Malvern Mastersizer 3,000 instrument with settings adapted from Jaijel et al. (2021), resulting in 101 size classes from 0.01 to 3,500 μm. Key parameters were calculated from the grain-size data following McCave and Andrews (2019), including mean size ($\overline{SS}$) and percentage ($SS\%$) of the sortable silt. We implemented end-member modeling for grain-size data with the AnalySize algorithm (Paterson & Heslop, 2015). The algorithm iteratively calculates the least-squares fit between the measured grain-size distribution and the calculated end-member mixture to approximate a theoretical distribution.

3. Results

3.1. Sortable Silt Systematics

At Site U1588, all samples consistently exhibit a bimodal grain-size distribution. The primary mode lies within the 5–8 μm range, with a minor peak around 1 μm (Figure 2c). A significant correlation ($r = 0.68$; $P < 0.01$) exists between the mean size ($\overline{SS}$) and percentage ($SS\%$) of the 10–63 μm sortable silt fraction (Figure 2d). Calculated $\overline{SS}$ values range from 15.3 to 18.4 μm, with $SS\%$ values between 17.1% and 34.7%.

The $\overline{SS}$ record of Site U1588 exhibits a precession cyclicity superimposed on the glacial-interglacial background (Figure 3c). Spectral analyses reveal a more pronounced ~21-kyr precession cyclicity when excluding the upper 60-ka interval (Figure 2e). The $\overline{SS}$ values are typically higher during precession maxima and lower during minima. Notably, during interglacial periods such as MIS 5 and 7, the $\overline{SS}$ record shows not only higher values but also larger variation amplitudes compared to those from glacial periods (e.g. MIS 6) (Figure 3c).

The calibrated $\overline{SS}$ grain-size flow speed proxy offers a quantitative framework to assess MOW modifications. The calibration equation: $\overline{SS} = 0.808 \times U + 15.46$ (where U = flow speed in cm/s and $\overline{SS}$ = mean sortable-silt size in μm), established through long-term current-meter observations across diverse hydrodynamic settings, is used (McCave et al., 2017). This approach is physically sound: Sites U1389 and U1588 are both located on drifts along the same MOW flow pathway (Hernández-Molina et al., 2014) (Figure 1c); and they share a clear cross-spectral correlation in precession cyclicity (Figure S8 in Supporting Information S1). For validation, the normalized difference is also quantified: $\Delta SS = \overline{SS}\ (U1389)_N - \overline{SS}\ (U1588)_N$. The reconstructed flow-speed record (ΔU, approximated by ΔSS) displays a pronounced precession cyclicity at 23 kyr (Figure 2f), with higher values corresponding to precession maxima and vice versa (Figure 3e). Superimposed on that, the ΔU record shows distinct glacial-interglacial trends over the last 250 kyr, with higher values during glacial periods (e.g. MIS 2–4 and 6) (Figure 3e).

3.2. End-Member Modeling

From the goodness-of-fit statistics (Figures 2a and 2b), the 3-EM model emerges as optimal, accounting for >85% of total variance while maintaining angular deviations of <1.5° ($n = 90$). The selection is further validated by the anomalous decrease in mean R^2 values when transitioning from 3-EM to 4-EM models (Figure 2a), indicating over-parameterization beyond three end-members.

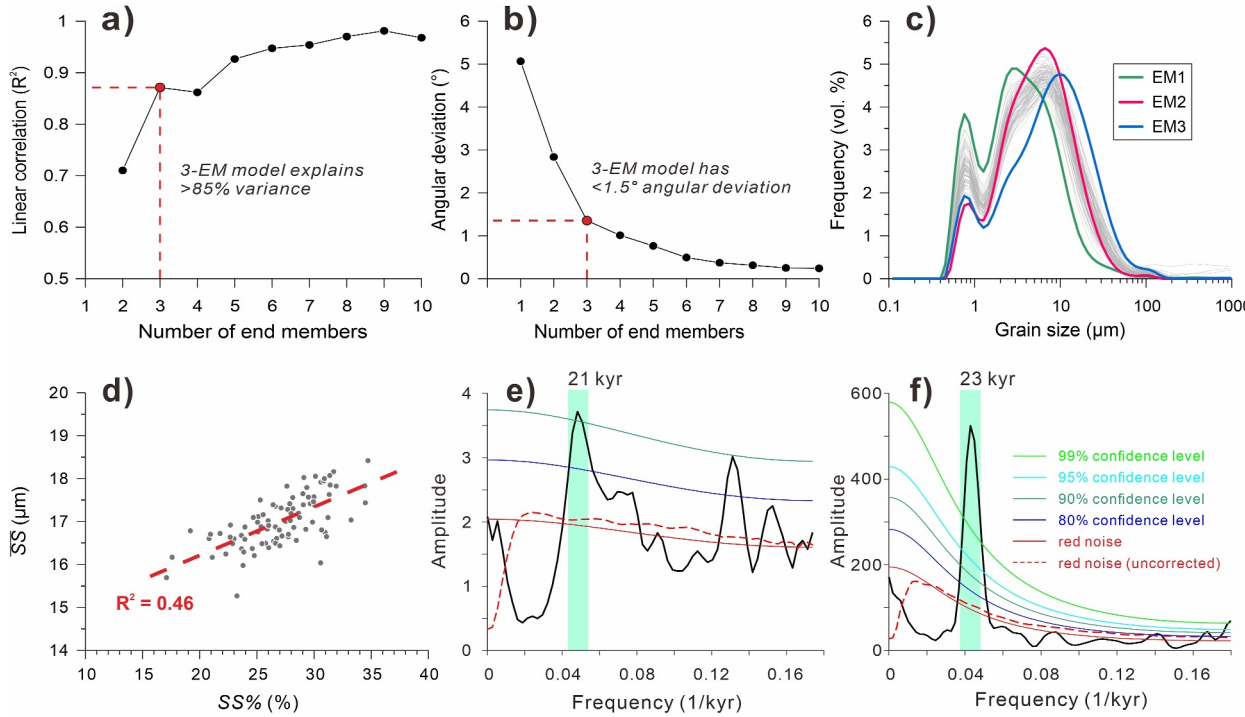

Figure 2. End-member modeling results and spectral analysis results of grain-size data at Site U1588. (a, b) Linear correlation and angular deviation for models with 2–10 end-members (Paterson & Heslop, 2015). The goodness-of-fit statistics suggest that the model with three end-members (3-EM model) is optimal, accounting for more than 85% of the variance (R^2) with less than 1.5° angular deviation. (c) Modeled grain-size distributions of the end members for the selected 3-EM model, displayed alongside those of all measured samples. (d) Significant correlation ($r = 0.68$; $P < 0.01$) exists between the mean size ($\overline{SS}$) and percentages ($SS\%$) of the terrigenous sortable silt fraction (10–63 μm). This suggests active size-dependent sorting under varying bottom-current shear stresses (McCave et al., 1995). (e) Spectrum of the $\overline{SS}$ record exhibits clear precession signals in MOW variability during Phase-I (~250–60 ka) at Site U1588. (f) Spectrum of the ΔU record (i.e., flow speed difference between Site U1389 and Site U1588; McCave and Andrews, 2019) shows a pronounced precession cyclicity, reflecting MOW's depth variations. The spectral analyses were performed by Redfit38 (Schulz & Mudelsee, 2002) with a Welch window (oversample: 6; segment: 3).

In the 3-EM model, the end-members show distinct grain-size distribution. EM1, EM2, and EM3 show the main mode at ~3, ~7, and ~12 μm, respectively, along with the common minor peak near 1 μm (Figure 2c). The relative proportions of EM1 and EM2 display generally opposite temporal patterns (Figure S5 in Supporting Information S1). EM3, representing ~5%–78% of total sediment composition, exhibits clear precession cycles overprinted on the glacial-interglacial background, which covaries with $\overline{SS}$ (Figure 3c). For validation of the grain size data, end-member modeling results and interpretations, refer to Supporting Information S1.

3.3. Benthic Foraminiferal $\delta^{18}O$ and $\delta^{13}C$

At Site U1588, the benthic foraminiferal $\delta^{18}O$ (2.06–4.80‰) exhibits a coherent pattern with nearby Site U1391 (Figure 3a); while the $\delta^{13}C$ record (−0.07–1.37‰) displays precession-like variations, with stronger expression during interglacial compared to glacial periods (Figure 3b).

4. Discussion

In the Gulf of Cadiz, near the Strait of Gibraltar, sediment grain-size distributions primarily reflect variations in bottom current velocity (de Castro et al., 2020). This is best exemplified by the successful application of SS proxy at Site U1389, presenting a high-resolution, 1-Ma long record of MOW flow strength variability (McCave, 2023). However, as MOW enters the Gulf of Cadiz and, by extension, the Iberian Margin, it can be traced along two distinct flow branches, each with a varying prevailing depth. This not only complicates the tracking of MOW but also raises the question of the extent to which SS can reflect the changes in MOW. Indeed, Site U1588 shows significantly lower $SS\%$ (25.9% ± 8.8%) compared to Site U1389 (38.3% ± 16.6%). This reduction likely reflects down-current fining within the lower MOW branch, indicative of decreased flow speed during northward transport—analogous to observations on the Gardar Drift (Bianchi & McCave, 2000).

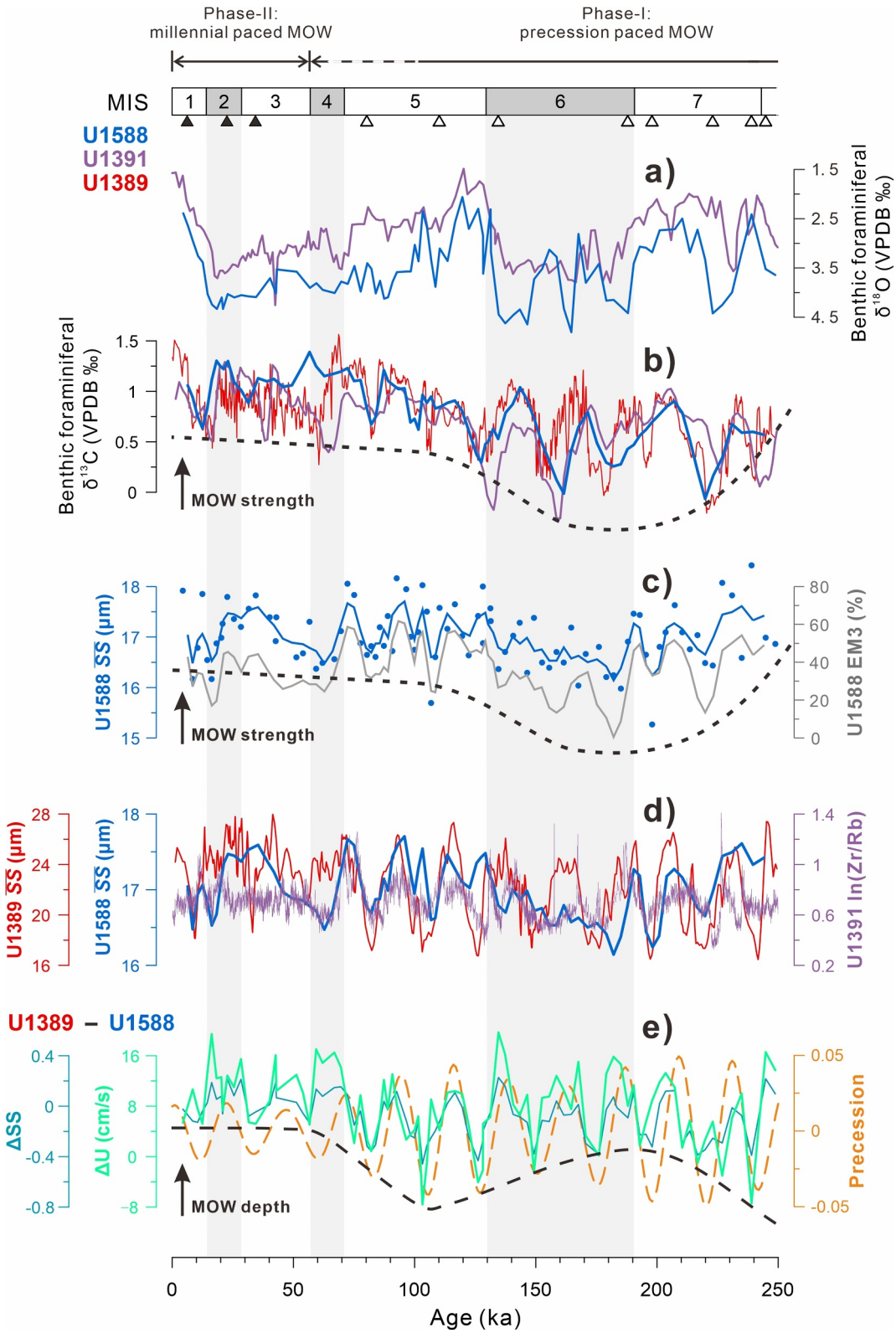

Figure 3.

Here, we explore whether the SS record at Site U1588 can reliably capture changes in MOW-related bottom-current dynamics (Section 4.1). We then examine the evolution of MOW in the lower branch over the last 250 kyr, focusing on orbital-scale variability and potential driving mechanisms (Section 4.2). Finally, we use the SS proxy systematics to estimate the flow speed difference between Sites U1389 and U1588, which we interpret as indicative of changes in the vertical structure of MOW during its northward transport (Section 4.3).

4.1. Sortable Silt as a Tracer of MOW Dynamics Changes

The terrigenous SS proxy exhibits inherent sensitivity to near-bottom current strength through two mechanisms (McCave et al., 1995). On the one hand, particles >10 μm, unlike finer cohesive sediments, respond to shear stress as discrete hydrodynamic units during the processes of erosion and deposition. This enables effective size sorting under varying current velocities. On the other hand, particles >63 μm show threshold transport behavior, requiring stronger currents for mobilization while simultaneously inhibiting the deposition of finer sediments under high flow regimes. Laboratory experiments and field investigations have confirmed a linear correlation between $\overline{SS}$ and bottom-current flow speed (McCave et al., 1995, 2017).

At Site U1588, the $\overline{SS}$ record robustly reflects MOW dynamics variations, as demonstrated through independent lines of evidence. Firstly, the good correlation ($r = 0.68$; $P < 0.01$) between the $\overline{SS}$ and $SS\%$ (Figure 2a) suggests active size-dependent sorting (McCave and Andrews, 2019). This confirms the SS proxy's sensitivity to MOW-mediated lateral transport at Site U1588, despite its reduced strength compared to the upstream Site U1389 along the northward pathway (Figure 1).

Moreover, there is a good covariation ($r = 0.83$; $P < 0.01$) between $\overline{SS}$ and EM3 component, showing precessional variability superimposed on a long-term trend (Figure 3c). Specifically, all terrigenous detrital samples exhibit consistent grain-size distributions, indicating a stable provenance pattern (Figure 2c). The optimal 3-EM model explains >85% variance, with <1.5° angular deviation. EM3, the coarsest component (~12 μm mode) constitutes ~5%–78% of the total variance and covaries with the $\overline{SS}$ record (Figure 3c). This covariation validates that SS proxy's reliability for reconstructing bottom-current dynamics, indicating sustained MOW influence at Site U1588 over the last 250 kyr. The sustained influence is confirmed by consistent benthic foraminiferal $\delta^{13}C$ variability at Sites U1389, U1391, and U1588, reflecting similar MOW-regulated ventilation (Figure 3b). As an ocean circulation tracer (Duplessy et al., 1988), benthic foraminiferal $\delta^{13}C$ records along MOW's northward pathway reveal an en-route dilution of precessional signals from the Mediterranean Sea to the high-latitude North Atlantic (Figure S10 in Supporting Information S1). Therefore, the multi-proxy validation, combined with established hydrodynamic principles, demonstrates SS systematics as a robust indicator of MOW dynamics variations for Site U1588 on the Iberian Margin, despite its relatively deep and distal location at the MOW northward pathway.

4.2. Two-Phase Evolution of MOW Over the Last 250 kyr

We present MOW strength records from three strategic locations and depths along its propagation route (Figures 1b and 1c). Site U1389 (644 m depth) in the Gulf of Cadiz, near the Strait of Gibraltar, serves as a reference record for the initial MOW intensity in the Atlantic. Further downstream, Sites U1391 (1,085 m depth) and U1588 (1,339 m depth), which are located successively farther north along the MOW pathway, can capture

Figure 3. Revealing northward depth fluctuations of the Mediterranean Outflow Water (MOW) over the last 250 kyr. (a, b) Benthic foraminiferal $\delta^{18}O$ and $\delta^{13}C$ records from Site U1389 (Sierro et al., 2020), Site U1391 (Guo et al., 2020) and Site U1588 (this study), respectively. (c) Strong covariation ($r = 0.83$; $P < 0.01$) exists between the mean size of sortable silt fraction ($\overline{SS}$) and the third component of optimal end-member model (EM3) for Site U1588. This demonstrates that the $\overline{SS}$ proxy record at Site U1588 reliably reflects MOW's strength variations (black dotted lines). Both raw data (dots) and 3-point moving average are presented. (d) MOW variability as recorded by $\overline{SS}$ proxy at Site U1389 (McCave, 2023) and Site U1588 (this study), and sedimentary ln(Zr/Rb) at Site U1391 (XRF core scanning data; Nichols et al., 2020). A two-phase evolution of MOW is revealed, transitioning from precession-dominated cycles to millennial-scale variability with reduced amplitude. (e) Flow speed difference (ΔU) between Sites U1389 and U1588 is calculated based on the calibrated $\overline{SS}$ grain-size flow speed proxy (McCave et al., 2017), reflecting MOW's depth fluctuations (black dashed line). Normalized index of $\overline{SS}$ difference (ΔSS) is also shown for validation. Both ΔU and ΔSS records show a strong precession cyclicity, and the amplitude variations follow the eccentricity-modulated climate precession (Laskar et al., 2004). This precession cyclicity reflects the mixing and dilution of MOW during its northward transport, suggesting a deeper MOW during precession maxima (Northern Hemisphere summer insolation minima), and vice versa. Vertical gray bands mark Marine Isotope Stage (MIS) (Lisiecki & Raymo, 2005). Black triangles (solid: ^{14}C dating; hollow: ^{18}O stratigraphy) denote tie-points of the age model (see Supporting Information S1).

depth-dependent modifications in bottom-current dynamics. Moreover, using the same calibrated $\overline{SS}$ grain-size flow speed proxy (McCave et al., 2017) allows us to quantify the difference in flow speeds between Site U1389 and Site U1588 (i.e., ΔU, confirmed by normalized ΔSS), which are respectively at the proximal and distal locations at the MOW northward pathway.

Despite the use of different proxy systems (e.g., terrigenous grain-size $\overline{SS}$, XRF core scanning ln(Zr/Rb), bulk sand% fraction), all three sites exhibit consistent patterns in the evolution of MOW (Guo et al., 2020; McCave, 2023; Nichols et al., 2020; Sierro et al., 2020). A phase shift is evident: precession cyclicity was prominent before ∼60 ka but almost muted afterward, giving way to millennial-scale variability (Figure 3d and Figure S9 in Supporting Information S1). This has been revealed by Nichols et al. (2020), via the anisotropy of magnetic susceptibility and sedimentary ln(Zr/Rb) records at Site U1391. This shift is more pronounced at Sites U1588 and U1391 compared to U1389, reflecting greater dilution of the precessional signals at downstream locations along MOW's transport pathway (Figure 3d and Figure S9 in Supporting Information S1). The stepwise evolution can also be seen from benthic foraminiferal $\delta^{13}C$ records at Site U1588, U1391, and U1389 (Figure 3b). Accordingly, the MOW evolution is divided into two phases, as follows.

During Phase-I (∼250–60 ka), the variability of MOW is dominated by precession cycles, with weaker MOW corresponding to precession minima and vice versa. At times of precession minima (i.e., Northern Hemisphere summer insolation maxima), more precipitation and runoff into the eastern Mediterranean Sea reduced its overturning circulation, suppressing the production of LIW (MOW's precursor). Besides the MOW strength shown by $\overline{SS}$ (Figures 3c and 3d), benthic foraminiferal $\delta^{13}C$ records, which reflect the MOW-mediated ventilation with respect to North Atlantic intermediate- to deep-waters, also reveal precession-paced variations in the Mediterranean freshwater budget (Figure 3b).

During Phase-II (∼60–0 ka), the changes in MOW appear to be out of phase with precessional cycles, and the variation amplitude is reduced compared to Phase-I. This is evident at the three sites presented here (Figure 3d) and other relevant sites in previous studies (Figure S10 in Supporting Information S1). It has been suggested that during this period, the flow strength of MOW was dominated by millennial-scale oscillations superimposed on orbitally driven changes (Bahr et al., 2015; Kaboth et al., 2016; Nichols et al., 2020).

4.3. Depth Variations of MOW During Northward Propagation

4.3.1. Deepening of MOW Since MIS 5

The en-route dilution of MOW is more pronounced during Phase-II than Phase-I, as indicated by phase offsets and different variability amplitudes (Figure 3d and Figure S9 in Supporting Information S1). In fact, the ΔU and ΔSS records suggest that this trend may have started as early as ∼100 ka (Figure 3e). The timing coincides with the termination of orbitally driven variability at the MIS 5/6 boundary, followed by the gradual emergence of millennial-scale variability during the MIS 4/5 transition and its full establishment by ∼60 ka. This pattern matches the magnetic susceptibility and sedimentary records of Site U1391 (Nichols et al., 2020) (Figure S9 in Supporting Information S1). We attribute this change to vertical migration of the MOW's prevailing depth and influence range, that is, a progressive deepening of MOW since ∼100 ka.

The observed deepening of MOW results from two main factors (Figure 4a). First, since MIS 4/5, the Heinrich Stadials became frequent and released massive meltwater from the Laurentide and Eurasian ice sheets (McManus et al., 1999). This should have caused reduced density of open North Atlantic waters relative to MOW, and thus a deeper settling depth of MOW (Rogerson et al., 2012; Sierro et al., 2020; Skinner & Elderfield, 2007).

Second, since MIS 3/4 when Greenland stadials were well-developed, strong cooling and aridification enhanced Mediterranean buoyancy loss, intensifying circulation (Cacho et al., 2006; Toucanne et al., 2012). This process strengthened LIW formation and produced denser MOW outflow (Rogerson et al., 2012), which was potentially augmented by increased Western Mediterranean Deep Water contributions (Voelker et al., 2006). Indeed, multi-proxy studies confirmed denser, deeper MOW along the Iberian Margin during these cold periods (Toucanne et al., 2007; van Dijk et al., 2018; Voelker et al., 2006). This is supported by the correlation between intensified LIW flow in the Mediterranean and MOW speed pulses along the Iberian slope (Figure S9 in Supporting Information S1). Although their relative contributions remain uncertain, these processes together explain the $\overline{SS}$ reduction at Site U1588 and increased ΔSS as reflecting MOW deepening rather than weakening (Figure 4a).

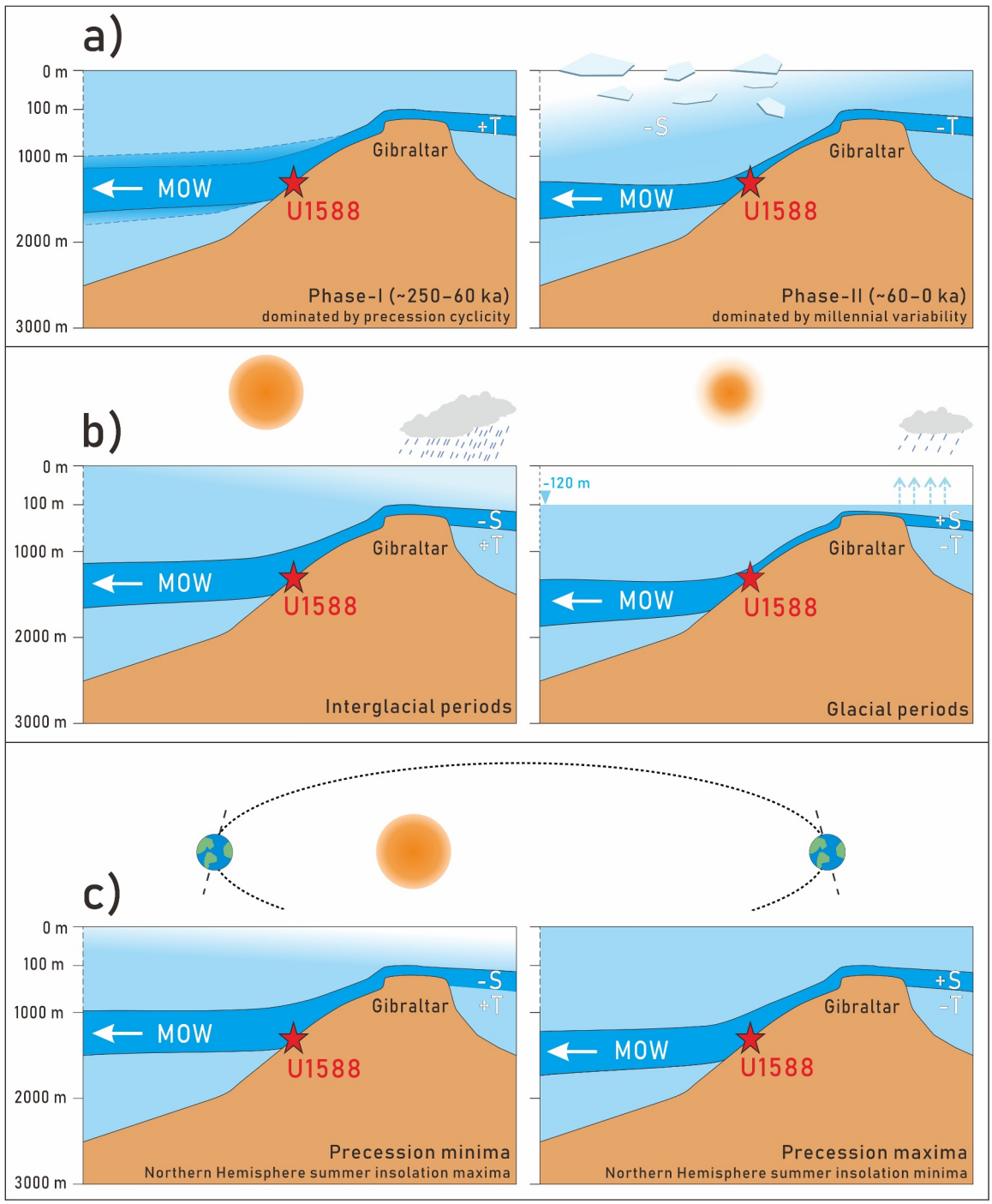

Figure 4. Northward depth fluctuations of the lower Mediterranean Outflow Water (MOW) on different timescales. (a) During precession-paced Phase-I (~250–60 ka), MOW occupied shallower depths than in Phase-II (~60–0 ka), which is dominated by millennial-scale climate variability (Figure 3e). The deepening of MOW during Phase-II results from reduced density of open North Atlantic waters due to massive iceberg melting during Heinrich Stadials, and/or enhanced production of more and denser MOW driven by Mediterranean regional cooling and aridification. (b) MOW's settling depth varied between glacial and interglacial periods (Figure 3e). During glacial times, a denser MOW deepened to below Site U1588 (1,339 m), while it shoaled and directly influenced Site U1588 sediments during interglacial periods, similar to the present-day situation (Figure 1c). (c) MOW's depth variability exhibits pronounced precession cycles, with amplitude modulated by eccentricity forcing (Figure 3e). At precession maxima when the flow intensified, MOW experienced more rapid mixing and dilution during its northward propagation. This en-route dilution is best attributed to increased density contrasts between MOW and ambient waters, indicating a deeper MOW at precession maxima (Northern Hemisphere summer insolation minima), and a shallower one otherwise. Abbreviation: S = salinity; T = temperature; +/− = increase/decrease.

4.3.2. Deeper MOW During Glacial Periods

On the glacial-interglacial timescale, vertical migration of MOW can explain the contrasting $\overline{SS}$ patterns between Sites U1588 and U1389 (Figure 3d). This suggests, beyond the Gulf of Cadiz, a depth-dependent MOW influence along its northward transport.

Given the denser glacial MOW suggested by various studies (Rogerson et al., 2005, 2012; van Dijk et al., 2018), this indicates that MOW's settling depth should have extended below Site U1588 (>1,339 m). This is supported by sedimentary, isotopic and ecological evidence, suggesting that the base of lower MOW could reach down to ∼2,000 m (Schönfeld & Zahn, 2000; Skinner & Elderfield, 2007). In contrast, during interglacial periods, MOW occupied shallower depths, directly influencing Site U1588, with its strength strongly paced by precession. This is confirmed by the present-day hydrographic observations, which represent the current interglacial, showing a distinct MOW salinity tongue at Site U1588 (Figure 1c).

This interpretation is supported by a closer coupling between benthic foraminiferal $\delta^{13}C$ and terrigenous $\overline{SS}$ during interglacial compared to glacial times, indicating MOW-regulated ventilation at Site U1588 (Figures 3b and 3c). This pattern is also observed at Site U1391 with similar depth and location to Site U1588 (Guo et al., 2017, 2020). The higher interglacial sensitivity is further evidenced by $\overline{SS}$ minima at ∼100 and ∼195 ka, coinciding with Mediterranean sapropel formation (Figure 3c). During these events, Mediterranean circulation collapsed, and strong water-column stratification resulted in extremely weak MOW (Rohling et al., 2015; J. Wu et al., 2019). Collectively, vertical migration and current strength, jointly control flow speed variability of MOW at Site U1588 on the glacial-interglacial timescale (Figure 4b).

4.3.3. Depth Fluctuations of MOW in Precession Cycles

The flow speed difference (ΔU, corroborated by normalized ΔSS) between Sites U1389 and U1588 exhibits a pronounced precession cyclicity over the last 250 kyr (Figure 2f). Both sites consistently record increased $\overline{SS}$ values during precession maxima (Northern Hemisphere summer insolation minima) and vice versa, reflecting orbitally driven variations in MOW strength (Figure 3e). However, the MOW intensification, as recorded by increased $\overline{SS}$ absolute values at both sites, simultaneously amplified the values of ΔU and ΔSS (Figure 3e). This demonstrates that during precession maxima, intensified MOW flow enhanced entrainment mixing and increased its dilution as it transported northward.

This dilution is best attributed to increased density contrasts between the lower MOW branch and ambient waters, consistent with modern observations (Baringer & Price, 1997; Copard et al., 2011; Sánchez-Leal et al., 2017). Given the well-established correlation between intensified MOW and elevated salinity/density (McCave, 2023; Rogerson et al., 2005, 2012; van Dijk et al., 2018), the increased flow-speed loss indicated by ΔU and ΔSS further suggests a deeper settling depth of MOW at precession maxima. Therefore, MOW's northward depth fluctuations covary with its strength, paced by precession (Figure 4c). Notably, the amplitudes of MOW's precession-driven depth variations appear to be modulated by eccentricity (Figure 3e).

Nevertheless, quantifying the relative contributions of depth versus strength to MOW variability is challenging, due to the bathymetric and hydrographic differences between sites. Furthermore, disentangling salinity and temperature effects to MOW settling depth variations remains unresolved. Temperature changes, as reflected in benthic foraminiferal $\delta^{18}O$ records, likely played a role, especially during MIS 6 (Figure 3a). These issues warrant systematic future investigations.

5. Conclusions

This study demonstrates terrigenous, non-cohesive sortable silt ($\overline{SS}$) as a robust hydrodynamic proxy at Site U1588 on the Iberian Margin, as corroborated by end-member modeling of grain-size data. By comparing two strategically located sites at diagnostic depths (U1389: 644 m vs. U1588: 1,339 m) along MOW's northward pathway, we implement a unified proxy framework based on $\overline{SS}$ systematics and benthic foraminiferal $\delta^{13}C$. This framework enables investigation of MOW's depth fluctuations over the last 250 kyr, as follows:

1. Terrigenous $\overline{SS}$ and benthic foraminiferal $\delta^{13}C$ records of Site U1588 reveal a two-phase evolution, with a transition occurred ∼100–60 ka. MOW gradually deepened from ∼100 to 60 ka, then stabilized—

synchronized with the development of millennial-scale climate variability. This deepening results from reduced density of open North Atlantic waters due to massive iceberg melting during Heinrich Stadials, and/or enhanced production of denser MOW driven by Mediterranean regional cooling and aridification.

2. Given a denser glacial MOW, the combination of absent glacial-interglacial cycles at Site U1389 and stronger precessional signals during interglacials than glacials at Site U1588, suggests that MOW's prevailing depth shifted to below Site U1588 (1,339 m) during glacial times. During interglacial periods, MOW shoaled and directly influenced Site U1588, with its flow strength strongly paced by precession.
3. Flow speed gradients between Sites U1389 and U1588 exhibit a pronounced precession cyclicity, suggesting that at precession maxima—when flow intensified—stronger mixing and dilution of MOW occurred during northward propagation. This en-route dilution is attributed to increased density contrasts between MOW and ambient waters, indicating deeper MOW penetration at precession maxima (Northern Hemisphere summer insolation minima), and vice versa.

Our findings reveal that precessional forcing regulates MOW's northward transport dynamics through both strength and depth variations, enabling low-to-high latitude climate signal transmission via temperature and salt transport.

Data Availability Statement

Data set for this research is available at J. Wu (2025).

Acknowledgments
This research used samples and data provided by the International Ocean Discovery Program (IODP). We thank the IODP Expeditions 397 crew, technicians, and scientists on board RV *JOIDES Resolution* for sampling and logistics support. Gratitude also goes to Zongxian He, Qin Deng, Xiaoying Jiang, and Mengli Cao for helping with laboratory work and analyses. We thank the two anonymous reviewers and editor Sarah Feakins for their constructive comments that improved the manuscript. This work is financially supported by the National Natural Science Foundation of China (42276051; 42306085; 42330403; 42176074), and Guangdong Basic and Applied Basic Research Foundation (2023A1515030293).

References

Abrantes, F., Hodell, D. A., Alvarez Zarikian, C. A., Brooks, H. L., Clark, W. B., Dauchy-Tric, L. F. B., et al. (2024). Site U1588. In D. A. Hodell, F. Abrantes, C. A. Alvarez Zarikian, & the Expedition 397 Scientists (Eds.), *Iberian Margin Paleoclimate*, *Proceedings of the International Ocean Discovery Program* (Vol. 397). (International Ocean Discovery Program). https://doi.org/10.14379/iodp.proc.397.106.2024

Bahr, A., Kaboth, S., Jiménez-Espejo, F. J., Sierro, F. J., Voelker, A. H. L., Lourens, L., et al. (2015). Persistent monsoonal forcing of Mediterranean Outflow Water dynamics during the late Pleistocene. *Geology*, *43*(11), 951–954. https://doi.org/10.1130/G37013.1

Baringer, M. O., & Price, J. F. (1997). Mixing and spreading of the Mediterranean outflow. *Journal of Physical Oceanography*, *27*(8), 1654–1677. https://doi.org/10.1175/1520-0485(1997)027<1654:MASOTM>2.0.CO;2

Bianchi, G. G., & McCave, I. N. (2000). Hydrography and sedimentation under the deep western boundary current on Björn and Gardar Drifts, Iceland Basin. *Marine Geology*, *165*(1–4), 137–169. https://doi.org/10.1016/S0025-3227(99)00139-5

Bigg, G. R., Jickells, T. D., Liss, P. S., & Osborn, T. J. (2003). The role of the oceans in climate. *International Journal of Climatology*, *23*(10), 1127–1159. https://doi.org/10.1002/jqs.599

Bower, A., Le Cann, B., Rossby, T., Zenk, W., Gould, J., Speer, K., et al. (2002). Directly measured mid-depth circulation in the northeastern North Atlantic Ocean. *Nature*, *419*(6907), 603–607. https://doi.org/10.1038/nature01078

Cacho, I., Shackleton, N., Elderfield, H., Sierro, F. J., & Grimalt, J. O. (2006). Glacial rapid variability in deep-water temperature and $\delta^{18}O$ from the Western Mediterranean Sea. *Quaternary Science Reviews*, *25*(23–24), 3294–3311. https://doi.org/10.1016/j.quascirev.2006.10.004

Catunda, M. C. A., Bahr, A., Kaboth-Bahr, S., Zhang, X., Foukal, N. P., & Friedrich, O. (2021). Subsurface heat channel drove sea surface warming in the high-latitude North Atlantic during the Mid-Pleistocene Transition. *Geophysical Research Letters*, *48*(11), e2020GL091899. https://doi.org/10.1029/2020GL091899

Cheng, X., Huang, B., Jian, Z., Zhao, Q., Tian, J., & Li, J. (2005). Foraminiferal isotopic evidence for monsoonal activity in the South China Sea: A present-LGM comparison. *Marine Micropaleontology*, *54*(1–2), 125–139. https://doi.org/10.1016/j.marmicro.2004.09.007

Colin, C., Duhamel, M., Siani, G., Dubois-Dauphin, Q., Ducassou, E., Liu, Z., et al. (2021). Changes in the intermediate water masses of the Mediterranean Sea during the last climatic cycle—New constraints from neodymium isotopes in foraminifera. *Paleoceanography and Paleoclimatology*, *36*(4), e2020PA004153. https://doi.org/10.1029/2020PA004153

Copard, K., Colin, C., Frank, N., Jeandel, C., Montero, S. J.-C., Reverdin, G., & Ferron, B. (2011). Nd isotopic composition of water masses and dilution of the Mediterranean outflow along South-West European margin. *Geochemistry, Geophysics, Geosystems*, *12*(6), Q06020. https://doi.org/10.1029/2011GC003529

de Castro, S., Hernández-Molina, F. J., Rodríguez-Tovar, F. J., Llave, E., Ng, Z. L., Nishida, N., & Mena, A. (2020). Contourites and bottom current reworked sands: Bed facies model and implications. *Marine Geology*, *428*, 106267. https://doi.org/10.1016/j.margeo.2020.106267

Dubois-Dauphin, Q., Colin, C., Bonneau, L., Montagna, P., Wu, Q., Van Rooij, D., et al. (2017). Fingerprinting Northeast Atlantic water masses using neodymium isotopes. *Geochimica et Cosmochimica Acta*, *210*, 267–288. https://doi.org/10.1016/j.gca.2017.04.002

Duplessy, J. C., Shackleton, N. J., Fairbanks, R. G., Labeyrie, L., Oppo, D., & Kallel, N. (1988). Deepwater source variations during the last climatic cycle and their impact on the global deepwater circulation. *Paleoceanography*, *3*, 343–360. https://doi.org/10.1029/PA003i003p00343

Guo, Q., Li, B., & Kim, J. K. (2017). Benthic foraminiferal assemblages and bottom water evolution off the Portuguese margin since the Middle Pleistocene. *Global and Planetary Change*, *150*, 94–108. https://doi.org/10.1016/j.gloplacha.2016.11.004

Guo, Q., Li, B., Voelker, A. H. L., & Kim, J. K. (2020). Mediterranean Outflow Water dynamics across the middle Pleistocene transition based on a 1.3 million-year benthic foraminiferal record off the Portuguese margin. *Quaternary Science Reviews*, *247*, 106567. https://doi.org/10.1016/j.quascirev.2020.106567

Hernández-Molina, F. J., Stow, D. A. V., Alvarez-Zarikian, C. A., Acton, G., Bahr, A., Balestra, B., et al. (2014). Onset of Mediterranean outflow into the North Atlantic. *Science*, *344*(6189), 1244–1250. https://doi.org/10.1126/science.1251306

Hodell, D. A., Abrantes, F., Alvarez Zarikian, C. A., Brooks, H. L., Clark, W. B., Dauchy-Tric, L. F. B., et al. (2024). Expedition 397 summary. In D. A. Hodell, F. Abrantes, C. A. Alvarez Zarikian, & the Expedition 397 Scientists (Eds.), *Iberian Margin Paleoclimate*, *Proceedings of the International Ocean Discovery Program* (Vol. 397). (International Ocean Discovery Program). https://doi.org/10.14379/iodp.proc.397.101.2024

Hodell, D. A., Crowhurst, S. J., Lourens, L., Margari, V., Nicolson, J., Rolfe, J. E., et al. (2023). A 1.5-million-year record of orbital and millennial climate variability in the North Atlantic. *Climate of the Past*, *19*(3), 607–636. https://doi.org/10.5194/cp-19-607-2023

Iorga, M. C., & Lozier, M. S. (1999). Signatures of the Mediterranean Outflow from a North Atlantic climatology: 1. Salinity and density fields. *Journal of Geophysical Research*, *104*(C11), 25985–26009. https://doi.org/10.1029/1999JC900115

Ivanovic, R. F., Valdes, P. J., Gregoire, L., Flecker, R., & Gutjahr, M. (2014). Sensitivity of modern climate to the presence, strength and salinity of Mediterranean-Atlantic exchange in a global general circulation model. *Climate Dynamics*, *42*(3–4), 859–877. https://doi.org/10.1007/s00382-013-1680-5

Jaijel, R., Goodman Tchernov, B. N., Biton, E., Weinstein, Y., & Katz, T. (2021). Optimizing a standard preparation procedure for grain size analysis of marine sediments by laser diffraction (MS-PT4SD: Marine sediments-pretreatment for size distribution). *Deep-Sea Research Part I*, *167*, 103429. https://doi.org/10.1016/j.dsr.2020.103429

Kaboth, S., Bahr, A., Reichart, G. J., Jacobs, B., & Lourens, L. J. (2016). New insights into upper MOW variability over the last 150 kyr from IODP 339 Site U1386 in the Gulf of Cadiz. *Marine Geology*, *377*, 136–145. https://doi.org/10.1016/j.margeo.2015.08.014

Kaboth, S., de Boer, B., Bahr, A., Zeeden, C., & Lourens, L. J. (2017). Mediterranean Outflow Water dynamics during the past ~570 kyr: Regional and global implications. *Paleoceanography*, *32*(6), 634–647. https://doi.org/10.1002/2016PA003063

Laskar, J., Robutel, P., Joutel, F., Gastineau, M., Correia, A. C. M., & Levrard, B. (2004). A long-term numerical solution for the insolation quantities of the Earth. *Astronomy and Astrophysics*, *428*(1), 261–285. https://doi.org/10.1051/0004-6361:20041335

Lisiecki, L. E., & Raymo, M. E. (2005). A Pliocene-Pleistocene stack of 57 globally distributed benthic $\delta^{18}O$ records. *Paleoceanography*, *20*, 1–17. https://doi.org/10.1029/2004PA001071

Lozier, M. S., & Stewart, N. M. (2008). On the temporally varying northward penetration of Mediterranean Overflow Water and eastward penetration of Labrador Sea Water. *Journal of Physical Oceanography*, *38*(9), 2097–2103. https://doi.org/10.1175/2008JPO3908.1

McCave, I. N., & Andrews, J. T. (2019). Distinguishing current effects in sediments delivered to the ocean by ice. I. Principles, methods and examples. *Quaternary Science Reviews*, *212*, 92–107. https://doi.org/10.1016/j.quascirev.2019.03.031

McCave, I. N. (2023). One million years of Mediterranean outflow strength. *Quaternary Science Reviews*, *317*, 108260. https://doi.org/10.1016/j.quascirev.2023.108260

McCave, I. N., Manighetti, B., & Beverldge, N. A. S. (1995). Circulation in the glacial North Atlantic inferred from grain-size measurements. *Nature*, *374*(6518), 149–152. https://doi.org/10.1038/374149a0

McCave, I. N., Thornalley, D. J. R., & Hall, I. R. (2017). Relation of sortable silt grain-size to deep-sea current speeds: Calibration of the "Mud Current Meter". *Deep-Sea Research Part I*, *127*, 1–12. https://doi.org/10.1016/j.dsr.2017.07.003

McManus, J. F., Oppo, D. W., & Cullen, J. L. (1999). A 0.5-million-year record of millennial-Scale climate variability in the North Atlantic. *Science*, *283*(5404), 971–975. https://doi.org/10.1126/science.283.5404.971

Millot, C. (2009). Another description of the Mediterranean Sea outflow. *Progress in Oceanography*, *82*(2), 101–124. https://doi.org/10.1016/j.pocean.2009.04.016

Nichols, M. D., Xuan, C., Crowhurst, S., Hodell, D. A., Richter, C., Acton, G. D., & Wilson, P. A. (2020). Climate-induced variability in Mediterranean Outflow to the North Atlantic Ocean during the Late Pleistocene. *Paleoceanography and Paleoclimatology*, *35*(9), e2020PA003947. https://doi.org/10.1029/2020PA003947

Paterson, G. A., & Heslop, D. (2015). New methods for unmixing sediment grain size data. *Geochemistry, Geophysics, Geosystems*, *16*(12), 4494–4506. https://doi.org/10.1002/2015GC006070

Reid, J. L. (1979). On the contribution of the Mediterranean Sea outflow to the Norwegian-Greenland Sea. *Deep-Sea Research*, *26*(11), 1199–1223. https://doi.org/10.1016/0198-0149(79)90064-5

Rogerson, M., Rohling, E. J., Bigg, G. R., & Ramirez, J. (2012). Paleoceanography of the Atlantic-Mediterranean exchange: Overview and first quantitative assessment of climatic forcing. *Review of Geophysics*, *50*(2), RG2003. https://doi.org/10.1029/2011RG000376

Rogerson, M., Rohling, E. J., Weaver, P. P. E., & Murray, J. W. (2005). Glacial to interglacial changes in the settling depth of the Mediterranean Outflow plume. *Paleoceanography*, *20*(3), PA3007. https://doi.org/10.1029/2004PA001106

Rohling, E. J., Marino, G., & Grant, K. M. (2015). Mediterranean climate and oceanography, and the periodic development of anoxic events (sapropels). *Earth-Science Reviews*, *143*, 62–97. https://doi.org/10.1016/j.earscirev.2015.01.008

Sánchez-Leal, R. F., Bellanco, M. J., Fernández-Salas, L. M., García-Lafuente, J., Gasser-Rubinat, M., César González-Pola, C., et al. (2017). The Mediterranean Overflow in the Gulf of Cadiz: A rugged journey. *Science Advances*, *3*(11), eaao0609. https://doi.org/10.1126/sciadv.aao0609

Schlitzer, R. (2022). Ocean data view [Software]. Retrieved from http://odv.awi.de

Schönfeld, J., & Zahn, R. (2000). Late Glacial to Holocene history of the Mediterranean outflow. Evidence from benthic foraminiferal assemblages and stable isotopes at the Portuguese margin. *Palaeogeography, Palaeoclimatology, Palaeoecology*, *159*(1–2), 85–111. https://doi.org/10.1016/S0031-0182(00)00035-3

Schulz, M., & Mudelsee, M. (2002). REDFIT: Estimating red-noise spectra directly from unevenly spaced paleoclimatic time series. *Computers & Geosciences*, *28*(3), 421–426. https://doi.org/10.1016/S0098-3004(01)00044-9

Shackleton, N. J., Hall, M. A., & Vincent, E. (2000). Phase relationships between millennial-scale events 64,000–24,000 years ago. *Paleoceanography*, *15*(6), 565–569. https://doi.org/10.1029/2000PA000513

Sierro, F. J., Hodell, D. A., Andersen, N., Azibeiro, L. A., Jimenez-Espejo, F. J., Bahr, A., et al. (2020). Mediterranean Overflow over the last 250 kyr: Freshwater forcing from the tropics to the ice sheets. *Paleoceanography and Paleoclimatology*, *35*(9), e2020PA003931. https://doi.org/10.1029/2020PA003931

Skinner, L. C., & Elderfield, H. (2007). Rapid fluctuations in the deep North Atlantic heat budget during the last glacial period. *Paleoceanography*, *22*(1), PA1205. https://doi.org/10.1029/2006PA001338

Swingedouw, D., Colin, C., Eynaud, F., Ayache, M., & Zaragosi, S. (2019). Impact of freshwater release in the Mediterranean Sea on the North Atlantic climate. *Climate Dynamics*, *53*(7–8), 3893–3915. https://doi.org/10.1007/s00382-019-04758-5

Toucanne, S., Jouet, G., Ducassou, E., Bassetti, M. A., Dennielou, B., Angue Minto'O, C. M., et al. (2012). A 130,000-year record of Levantine Intermediate Water flow variability in the Corsica Trough, western Mediterranean Sea. *Quaternary Science Reviews*, *33*, 55–73. https://doi.org/10.1016/j.quascirev.2011.11.020

Toucanne, S., Mulder, T., Schönfeld, J., Hanquiez, V., Gonthier, E., Duprat, J., et al. (2007). Contourites of the Gulf of Cadiz: A high-resolution record of the paleocirculation of the Mediterranean outflow water during the last 50,000 years. *Palaeogeography, Palaeoclimatology, Palaeoecology*, *246*(2–4), 354–366. https://doi.org/10.1016/j.palaeo.2006.10.007

van Dijk, J., Ziegler, M., de Nooijer, L. J., Reichart, G. J., Xuan, C., Ducassou, E., et al. (2018). A Saltier Glacial Mediterranean Outflow. *Paleoceanography and Paleoclimatology*, *33*(2), 179–197. https://doi.org/10.1002/2017PA003228

Voelker, A. H. L., Lebreiro, S. M., Schönfeld, J., Cacho, I., Erlenkeuser, H., & Abrantes, F. (2006). Mediterranean outflow strengthening during northern hemisphere coolings: A salt source for the glacial Atlantic? *Earth and Planetary Science Letters*, *245*(1–2), 39–55. https://doi.org/10.1016/j.epsl.2006.03.014

Wu, J. (2025). Dataset: Depth fluctuations of Mediterranean Outflow Water along its northward propagation. *Zenodo*. https://doi.org/10.5281/zenodo.15375707

Wu, J., Liu, Z., Stuut, J. B. W., Zhao, Y., Schirone, A., & de Lange, G. J. (2017). North-African paleodrainage discharges to the central Mediterranean during the last 18,000 years: A multiproxy characterization. *Quaternary Science Reviews*, *163*, 95–113. https://doi.org/10.1016/j.quascirev.2017.03.015

Wu, J., Pahnke, K., Böning, P., Wu, L., Michard, A., & De Lange, G. J. (2019). Divergent Mediterranean seawater circulation during Holocene sapropel formation—Reconstructed using Nd isotopes in fish debris and foraminifera. *Earth and Planetary Science Letters*, *511*, 141–153. https://doi.org/10.1016/j.epsl.2019.01.036

Wu, W., Danabasoglu, G., & Large, W. G. (2007). On the effects of parameterized Mediterranean overflow on North Atlantic Ocean circulation and climate. *Ocean Modelling*, *19*(1–2), 31–52. https://doi.org/10.1016/j.ocemod.2007.06.003

Zweng, M. M., Reagan, J. R., Seidov, D., Boyer, T. P., Locarnini, R. A., Garcia, H. E., et al. (2018). World Ocean Atlas 2018 Volume 2: Salinity [Dataset]. In A. Mishonov Technical (Ed.), *NOAA Atlas NESDIS* (Vol. *82*, p. 50). https://doi.org/10.25923/9pgv-1224

References From the Supporting Information

Abrantes, F., Lebreiro, S., Rodrigues, T., Gil, I., Bartels-Jónsdóttir, H., Oliveira, P., et al. (2005). Shallow-marine sediment cores record climate variability and earthquake activity off Lisbon (Portugal) for the last 2000 years. *Quaternary Science Reviews*, *24*(23–24), 2477–2494. https://doi.org/10.1016/j.quascirev.2004.04.009

Fabian, S. G., Gallagher, S. J., & De Vleeschouwer, D. (2025). Benthic foraminiferal population dynamics at the Goban Spur off Southwest Ireland reveal glacial-interglacial bottom water ventilation and organic flux variability over the last 420,000 years. *Marine Micropaleontology*, *194*, 102432. https://doi.org/10.1016/j.marmicro.2024.102432

Heaton, T. J., Köhler, P., Butzin, M., Bard, E., Reimer, R. W., Austin, W. E. N., et al. (2020). Marine20—The Marine radiocarbon age calibration curve (0–55,000 cal BP). *Radiocarbon*, *62*(4), 779–820. https://doi.org/10.1017/RDC.2020.68

Hodell, D. A., & Channell, J. E. T. (2016). Mode transitions in Northern Hemisphere glaciation: Co-evolution of millennial and orbital variability in Quaternary climate. *Climate of the Past*, *12*(9), 1805–1828. https://doi.org/10.5194/cp-12-1805-2016

Hoogakker, B., Elderfield, H., Oliver, K., & Crowhurst, S. (2010). Benthic foraminiferal oxygen isotope offsets over the last glacial-interglacial cycle. *Paleoceanography*, *25*(4), PA4229. https://doi.org/10.1029/2009PA001870

Howell, P., Pisias, N., Balance, J., Baughman, J., & Ochs, L. (2006). ARAND time-series analysis software [Software]. *Brown University, Providence RI*. Retrieved from https://github.com/jesstierney/arand

Li, M., Hinnov, L. A., & Kump, L. R. (2019). Acycle: Time-series analysis software for paleoclimate research and education. *Computers & Geosciences*, *127*, 12–22. https://doi.org/10.1016/j.cageo.2019.02.011

Stuiver, M., & Reimer, P. J. (1993). Extended ^{14}C data base and revised CALIB 3.0 ^{14}C age calibration program. *Radiocarbon*, *35*(1), 215–230. https://doi.org/10.1017/S0033822200013904

Wang, P., Tian, J., & Lourens, L. J. (2010). Obscuring of long eccentricity cyclicity in Pleistocene oceanic carbon isotope records. *Earth and Planetary Science Letters*, *290*(3–4), 319–330. https://doi.org/10.1016/j.epsl.2009.12.028

Weltje, G. J. (1997). End-member modeling of compositional data: Numerical-statistical algorithms for solving the explicit mixing problem. *Mathematical Geology*, *29*(4), 503–549. https://doi.org/10.1007/BF02775085